

## Visualisation of multiple vortex rings from an axisymmetric synthetic jet

C. Fischer and R. Sharma

Department of Mechanical Engineering  
University of Auckland, Auckland 1142, New Zealand

### Abstract

Synthetic jets have been an area of interest in the recent years with constantly increasing industrial demand. Application areas are widespread and a strong focus is put on boundary layer control as well as on mixing enhancement. A synthetic jet has been studied using physical experiments involving high-speed camera footage and smoke visualisation. Additionally, three-dimensional transient numerical simulations have been performed. In the physical experiments high-speed camera footage is used to capture the smoke visualisation of the synthetic jet flow field where vortex interaction was present. The hybrid turbulence model SAS (ANSYS CFX) is used for the numerical simulations. The results of the numerical simulations show good visual agreement in the jet flow field.

### Introduction

A common synthetic jet actuator (SJA) usually consists of an oscillating membrane opposite the orifice in a cavity. Actuators can be pistons, piezo-electric disks, or loudspeakers. The volume and shape of both the cavity and the orifice vary largely, including round, square, and rectangular shapes. During a cycle, the oscillating membrane moves up and down, usually in a sinusoidal motion, pushing ambient air out of and sucking air into the cavity. During the expulsion part of the cycle, vortex rings and vortical structures can roll-up and move away from the orifice creating a synthetic jet (SJ). The shape and size of these vortical structures depend on the orifice geometry and on the actuator settings. Vortex roll-up is ensured if certain criteria are fulfilled. Initial conditions such as operating frequency, amplitude, cavity volume, orifice shape, etc. vary largely in the different studies presented in the literature. These initial conditions strongly influence the jet flow field and hence there is still limited information in terms of vortex formation, but more over in vortex interaction.

There are two types of SJ: 1) axisymmetric or three-dimensional (3D) jets created from a round orifice and 2) planar or two-dimensional (2D) jets created from rectangular orifices. The SJ is developed from ambient air and thus the net mass flux over a cycle is zero. Therefore, the SJ is also referred to as a zero-net-mass-flux jet. This property has an advantage over a continuous jet that does need an additional fluid supply, which makes the SJ attractive for numerous applications.

SJs have been an area of interest for a few decades now with constantly increasing industrial demand in the recent years. Application areas include flow separation control, cooling, thrust vectoring, and sound emission reduction. However, a strong focus has been put on boundary layer control [1, 4, 9] and fluid mixing applications, including heat transfer [3, 6, 8].

Computational Fluid Dynamics (CFD) have been utilised for SJ flow studies to get detailed flow field information, which is often limited in physical experiments. In this work, flow visualisation

was used to identify vortical structures and for comparison with visualisation tools from numerical simulations.

For the numerical simulations, the hybrid Unsteady Reynolds Averaged Navier–Stokes (URANS) turbulence model - Scale Adaptive Simulation-Shear Stress Transport (SAS-SST) - was used in this study. Standard two-equation turbulence models fail to predict complex 3D flows, such as of the SJ, whereas Large Eddy Simulations (LES) or Direct Numerical Simulations (DNS) demand high computational resources. Therefore, the hybrid model was chosen and its capability to resolve the jet flow is presented.

### Experimental Setup

#### Actuator Properties

The actuator used in this research was an 8” woofer with a frequency range of 38Hz-4.5KHz. Operating frequency of the woofer was  $f_d=40$ Hz. The woofer amplitude was kept constant by measuring the diaphragm displacement with a laser vibrometer during the experiment. A function generator and an amplifier drove the woofer. The case presented in this paper utilises a round orifice with a diameter of  $d_o=20$ mm and an orifice plate thickness of  $l_o=9$ mm. The cavity depth was  $h_c=100$ mm and the cavity volume was  $27 \times 10^5 \text{mm}^3$ . Based on the definitions of Smith and Glezer [7] the presented data of experimental setup resulted in  $S=81$ ,  $L=8.6$  and  $Re_d=18\,000$ .

#### High-Speed Camera

The Olympus i-SPEED 2 high-speed video camera was used for the flow visualisation. Camera software was used to analyse and evaluate the pictures which were compared to numerical simulation data. The minimum camera frame rate was 60fps at 800x600 pixel resolution. The maximum camera frame rate was 33 000fps which resulted in a minimum image size of 96x72 pixel.

Different camera settings were trialled to find a reasonable picture quality. The challenge lay in finding a proper frame rate and a high illumination at the same time. Table 1 shows the available mode of the high-speed camera.

Frame rate in fps	Exposure time in $\mu$ s	Image resolution (14 $\mu$ m pixel size)
800	1200	800 x 600
1000	1000	800 x 600
1000	500	800 x 600
1500	666	672 x 504
1500	333	672 x 504
1500	133	672 x 504
2000	500	576 x 432
2000	250	576 x 432

Table 1. Camera settings used during the visualisation experiments [5].

The brightest pictures were taken at a frame rate of 800fps. Using this setting also had the advantage that the picture size was

greatest (800x600). However, this setting did not quite capture the jet flow because of the low frame rate; only 20 pictures per jet-cycle ( $f_d=40\text{Hz}$ ). An addition, reducing the exposure time lead to a higher picture quality and the picture was less blurry but a lower exposure time also resulted in a darker picture. Obviously, the highest frame rate with a small exposure time was desirable and in the end, the optimum setting was found to be 2000fps with an exposure time of  $500\mu\text{s}$ .

### Smoke Machine

The most popular flow visualisation in air is the usage of smoke. The usage of incense sticks was tried in an earlier set of experiments. However, it was observed that the amount of generated smoke was insufficient for proper visualisation. Furthermore, the usage of more than one stick questioned the interruption level of the incense stick on the flow field inside the cavity and also of the flow development outside the cavity.

The alternative was the usage of a smoke machine. The machine can either be connected to the cavity to fill it up with smoke or a small tube can be used to inject smoke outside the cavity in the vicinity of the orifice exit. For each run the cavity was filled up with smoke using a funnel. The main objective was the usage of a non-toxic, non-irritating, environmentally friendly and non-flammable fluid which created a high reflective smoke. This smoke also had to have a particle size of around  $0.5\mu\text{m}$  to prevent it from significantly affecting the flow field. Thus, a widely used hydrocarbon oil was vaporized and then added to the flow. The smoke machine used was a 400W Vaperiza400 Fogger with a flow rate of  $1250\text{ft}^3/\text{min}$  ( $0.59\text{m}^3/\text{s}$ ).

### Lighting

For lighting, a Philips Pacific 23°-50° Zoomspot with a 1000W lamp (240V) was used. Light shades of the spotlight were used to create a light plane as thin as possible. Therefore, the light was concentrated in one plane and allowed for 2D, cut-plane like, pictures.

### **Numerical Setup**

The hybrid URANS model SAS-SST (ANSYS CFX 13, model version 2005) was used for the numerical simulations. The actuator was moving in a sinusoidal motion using an expression function. The movement of the “rubber” ring around the diaphragm was unspecified thus allowing for the movement. All other parts in the domain were kept stationary. The domain above the orifice was a cube with  $20d_o$  edge length. The outlets around the orifice were defined as openings (OPa relative pressure) with low turbulence intensity (1%). The outlet at the top was also defined as an opening (OPa relative pressure) but with high turbulence intensity (10%). The orifice plate, the cavity neck and all remaining parts inside the cavity were defined as no slip walls. The fluid used was “Air Ideal Gas” at  $21^\circ\text{C}$ . The convergence criteria was set to  $\text{RMS}=1\times 10^{-5}$ . The selected time step size of  $t_{\text{step}}=T/2000$  ( $T=1/f_d$ ) resulted in a maximum Courant number smaller than one. The High Resolution advection scheme and a second order backward Euler transient scheme were used. The solver was run in double precision and all remaining settings were kept as default. The mesh used in these simulations was built in ICFM CFD. It was a block structured hexahedral mesh consisting of  $3.8\times 10^6$  nodes.

### Visualisation Tools

Popular ways to visualise vortex core regions in CFD are types of the second invariant of the velocity gradient tensor, such as  $Q$ -criterion, swirling strength or Lambda 2-criterion etc. Other methods to identify vortices are vorticity, vector plots,

streamlines or low-pressure areas. The method used in this research was the  $Q$ -criterion.

For more details on the numerical simulations used in the present research the reader is referred to [2], e.g. for mesh and time step size studies and for comparison of different turbulence models.

### **Results**

Figure 1-3 show comparison of experimental and numerical data of visualisation of multiple vortex rings during one cycle. Three stages of the jet during a cycle are shown. The pictures taken from the physical and numerical experiments did not always match exactly the same time spot during the cycle. However, closest moments judged by visual agreement were taken for comparison. The pictures on top were taken from the smoke visualisation and the pictures at the bottom of each figure show the  $Q$ -criterion from the numerical simulations. The pictures taken from the numerical experiments also show the velocity in the flow direction where yellow indicates high velocities and blue indicates low velocities. The flow is from right to left in all pictures.

The first set of pictures (Figure 1) show the primary vortex ring followed by a secondary ring at middle of the expulsion cycle. The primary vortex was the biggest in size compared to all following vortices in a cycle. The primary ring developed at the edge of the orifice in the beginning of the expulsion part of the cycle. Once the primary ring had grown to a certain size, it detached from the orifice plate and moved away. In contrast, all following vortex rings were smaller and developed from the shear layer within the jet.

The sizes of the vortex rings from the numerical simulation were slightly smaller compared to the physical experiment. The ring sizes were estimated by calculating the jet half-width at different locations downstream of the orifice exit [2].

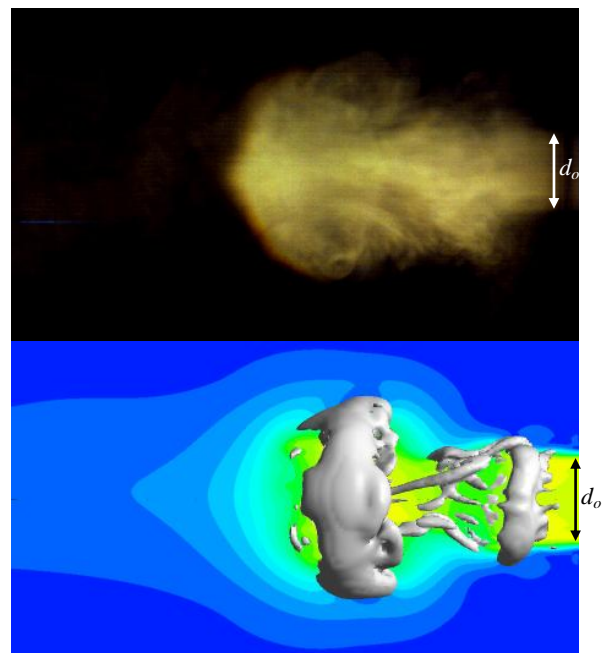


Figure 1. SJ in the middle of the expulsion part of the cycle.  $t=0.01562\text{s}$  in the numerical simulation (0.025 is a full cycle).

Soon after the second vortex ring had developed, it was influenced by the first vortex. The primary ring grew in size thereby decelerated, whereas the following vortex was accelerated and remained almost constant in size. This can be

seen in Figure 2. The second ring was deformed and had an outer diameter smaller than the inner diameter of the primary ring. The yellow area in the CFD picture (bottom of Figure 2) indicated that the second ring had a higher velocity than the primary ring. Thus, the second ring was able to undergo the first ring. This phenomenon is referred to as leapfrogging. After leapfrogging the second vortex merged with the first one and further downstream the merged rings got unstable.

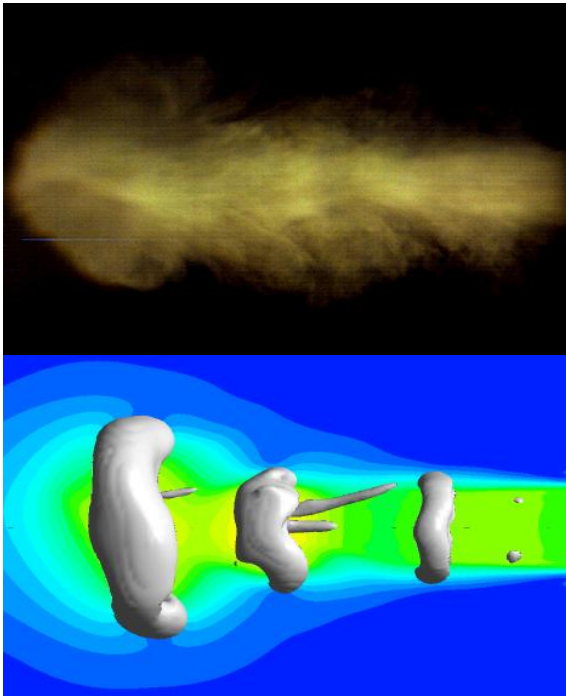


Figure 2. SJ in the end of expulsion part of the cycle.  $t=0.01875s$  in the numerical simulation.

The third vortex ring was little influenced by the flow upstream but instead influenced by the flow downstream. Figure 3 shows the third vortex ring in the end of the whole cycle and it can be seen that part of the smoke was sucked back into the cavity (top of Figure 3). This ring was originally in size of the second ring and grew a little in size before getting unstable. The third smoke ring quickly diminished by reaching the end of the observed flow region.

## Conclusions

A SJ flow field at a Reynolds number of  $Re_d=18\,000$  has been investigated experimentally and numerically. High-speed camera footage of smoke visualisation has been compared to CFD data using the hybrid turbulence model SAS. Visualisation of the jet revealed vortex dynamics resulting from the initial SJA conditions investigated in this paper. The comparison of experimental and numerical data showed visual agreement in vortex core region of the jet flow field. The SAS model was able to resolve the turbulent flow to some degree as the complex vortex dynamics present in the jet flow field could be reproduced. This gives confidence in using the hybrid turbulence model to compute SJ flows. Instead of using intensive models such as LES or DNS the SAS model can be used as a potential tool to study flow phenomena such as leapfrogging.

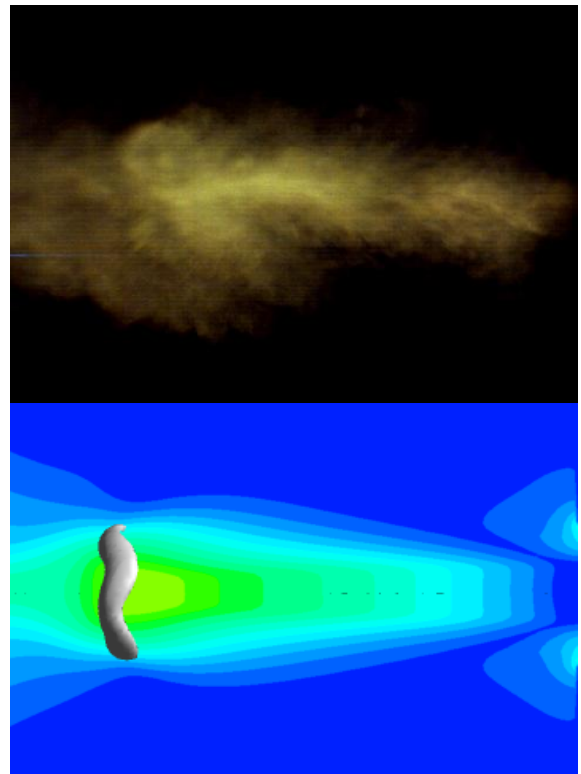


Figure 3. SJ during the ingestion part of the cycle.  $t=0.021875s$  in the numerical simulation.

## References

- [1] Dandois, J. and Garnier, E., Unsteady simulation of a synthetic jet in a cross-flow, *AIAA Journal*, **44**, No. 2, 2006, 225–238.
- [2] Fischer, C. and Sharma, R.N., Transitional Synthetic Jet from a Round Orifice: 3D Numerical Simulation of Leapfrogging and Vortex Ring Interaction using a Hybrid Turbulence Model, *ISTP-23*, Auckland, New Zealand, 19–22 November 2012.
- [3] Gillespie, M.B., Black, W.Z., Rinehart, C. and Glezer, A., Local convective heat transfer from a constant heat flux flat plate cooled by synthetic air jets, *J. Heat Transfer*, **128**, Iss. 10, 2006, 990–1000.
- [4] Gordon, M., Cater, J.E. and Soria, J., Investigation of the mean passive scalar field in zero-net-mass-flux jets in cross-flow using planar-laser-induced fluorescence, *Physics of Fluids*, **16**, No. 3, 2004, 794–808.
- [5] Olympus Product Guide, Olympus i-SPEED 2.
- [6] Pavlova, A. and Amitay, M., Electronic cooling using synthetic jet impingement, *J. Heat Transfer*, **128**, 2006, 897–907.
- [7] Smith, D.R. and Glezer, A., The formation and evolution of synthetic jets, *Physics of Fluids*, Vol. **10**, No. 9, 1998, 2281–2297.
- [8] Trávníček, Z. and Tesař, V., Annular synthetic jet used for impinging flow mass-transfer, *Int. J. Heat Mass Transfer*, **46**, 2003, 3291–3297.
- [9] Zhong, S., Millet, F. and Wood, N.J., The behaviour of circular synthetic jets in a laminar boundary layer, *Aeronautical J.*, **109**, No. 1100, 2005, 461–470.